Microstructure and mechanical properties of laser deposition manufactured a newly developed Ti-6Al-2Mo-2Sn-2Zr-2Cr-2V titanium alloy

Chao Wang
Junzhen Yi (jzyi@sau.edu.cn)
Shenyang Aerospace University
Jiaxing Wang
Jiabao Wu
Shuai Shao
Lanyun Qin
Guang Yang

Research Article

Keywords: Laser deposition manufacturing, Titanium alloy, Microstructure, Mechanical property, Heat treatment

Posted Date: March 30th, 2022

DOI: https://doi.org/10.21203/rs.3.rs-1431122/v1

Abstract

With the rapid development of aviation industry, the study of new type titanium alloy with superior mechanical properties is of great significance. In this paper, a newly developed Ti-6Al-2Mo-2Sn-2Zr-2Cr-2V (Ti-622222) alloy was fabricated by laser deposition manufacturing (LDM). The as-deposited Ti-622222 alloy exhibits coarse β columnar grains containing the basket-weave structure knitted with α phases and β phases. The solution and aging treatment decreases the size and content of primary α phase, but promotes the precipitation of secondary α phase. The microhardness shows a rising trend with the solution temperature increasing due to the precipitation of fine secondary α phase. The LDMed Ti-622222 alloy exhibits superior tensile strength (1025 MPa) and inferior elongation (6.0%). With the solution temperature increasing, the strength increases but the plasticity first increases and then decreases. The LDMed Ti-622222 alloy exhibits a mixed fracture mechanism of ductile and brittle fracture. The LDMed Ti-622222 alloy exhibits obvious anisotropy of impact property, the average impact toughness of the as-deposited sample in scanning direction is 23.4 J/cm^2 lower than that (40.9 J/cm^2) in deposition direction. After solution and aging treatment, the impact toughness improves significantly. With the solution temperature increasing, impact toughness first increases and then decreases.

1 Introduction

Titanium (Ti) alloys has been widely used in aerospace field due to its good comprehensive mechanical properties of strength-to-density ratio, toughness, creep resistance, corrosion resistance and thermal stability at room and elevated temperatures. Due to the rapid development of aerospace industry and the harsh working environment, the higher mechanical property requirements are put forward for Ti alloys, especially for the strength and toughness [1, 2]. In this case, the traditional Ti alloy has been unable to meet the mechanical property requirement of aerospace parts, so the new Ti alloys with high strength and high toughness need to be developed.

High strength and high toughness Ti alloys, which normally exhibits phase composition of near-beta (β) state, are generally characterized by high tensile strength, excellent plasticity and fracture toughness [3, 4]. In recent decades, many researchers have focused on the research of high strength and high toughness Ti alloy and many types of new alloys have been developed. Ti-10V-2Fe-3Al (Ti-1023) alloy is one of the most widely used near β titanium alloys with high strength and high toughness [5, 6]. Studies have shown that the solution and aging treatment can further improve the mechanical properties of the Ti-1023 alloy, making the strength and toughness match well [7]. In addition, researchers further found that the control of Fe content (≈2%) and O content (≈0.13%) can improve the forging performance and fracture toughness of Ti-1023 alloy [8]. Ti-5Al-5Mo-5V-1Fe-1Cr (BT22) alloy, which exhibits superior comprehensive mechanical properties and weldability [9], is also widely used in the production of aircraft body [10]. Its tensile strength can be significantly improved by using the solution and aging heat treatment [11]. Ti-5Al-5Mo-1V-1Cr-1Fe-1.5Sn-2Zr (BT22M) alloy, improving BT22 alloy by adding Sn and Zr, exhibits superior room temperature tensile strength (1200–1350 MPa), fracture toughness (54 MPa·m$^{1/2}$) and can keep stability of mechanical properties at 400 ℃ [12]. In addition, based on BT22

alloy, researchers successively developed Ti-5Al-5Mo-5V-3Cr-0.5Fe (Ti5553) alloy [13] and Ti-5Al-5Mo-5V-3Cr-0.6Fe (Timetal555) [14] alloy with less Fe content, which both showed a good match between strength and toughness. Although the available Ti alloys have been exhibited excellent comprehensive properties, it is still not enough to meet the processing and mechanical property requirements for structural components applied in aerocraft. It still deserves serious concern for the development of new Ti alloy with high strength and high toughness.

Traditionally, it cost much for the Ti alloys structural components due to the complex preparation process involving a sequence of hot working and machining processes [15]. In addition, higher requirements for the preparation process are put forward to meet the design concept of lightweight, complication and integration for Ti alloy components with the rapid development of aerospace industry. Laser deposition manufacturing (LDM) is an integrated forming manufacturing technology with high efficiency, high precision and low cost [16–18], which provides a novel manufacturing approach for Ti alloy components with complex configuration. In recent years, the correlation studies focused on the applications of LDM technique in high strength and high toughness Ti alloys have been widely carried out, such as Ti-5Al-2Sn-2Zr-4Mo-4Cr alloy [19], Ti-5Al-5Mo-5V-3Cr alloy [20], Ti-5Al-5Mo-5V-1Cr-1Fe alloy [21–23], Ti-5Al-5Mo-5V-3Cr-1Zr alloy [24, 25], and Ti-5Al-2Sn-2Zr-4Mo-4Cr alloy [26]. For high strength and high toughness Ti alloys, the LDM preparation process involves a complex nonequilibrium physical and unconventional metallurgical nature, which is still full of uncertainties. Therefore, it deserves more investigations focusing on the LDMed Ti alloys with high strength and high toughness to explore the feasibility of LDM process in fabricating the high strength and high toughness Ti alloys.

In this paper, a new-type high strength and high toughness Ti-6Al-2Mo-2Sn-2Zr-2Cr-2V (Ti-622222) alloy was fabricated by the LDM technology. The microstructure and mechanical properties of LDMed Ti-622222 alloy were deeply studied, and the anisotropy of mechanical properties was also investigated. In addition, to further improve the mechanical properties of as-deposited Ti-622222 alloy, the solution and aging heat-treatment with different temperatures was carried out, and the effect of solution temperature on microstructure and mechanical properties of LDMed Ti-622222 alloy was also investigated.

2 Experimental

In this work, the forged Ti-6Al-4V alloy thick plate was selected as the experimental substrate, and its chemical composition was shown in Table 1. Prior to the LDM test, the surface of the substrate was ground with SiC papers, and then was cleaned in alcohol and dried in air to ensure the substrate surface was clean. The raw material used for LDM test was self-developed Ti-6Al-2Mo-2Sn-2Zr-2Cr-2V (Ti-622222) alloy powder with the chemical composition listed in Table 1. The spherical alloy powder was prepared by gas atomization method with the particle size of 80–100 mesh. The alloy was designed on the basis of Ti-6Al-4V alloy by adding the elements of Mo, Cr, Sn and Zr. The optimal addition of Mo and Cr elements can improve the strength and plasticity of Ti alloy by the fine grain strengthening effect [27]. The Sn and Zr elements were added to improve the strength by solution strengthening effect and keep the

mechanical properties stable at high operation temperature [27, 28]. In order to ensure the quality of LDMed sample, the alloy powder was conducted vacuum drying for 4 h at 120 ℃ before the LDM test.

Table 1
Chemical composition of materials used in this work (wt. %)

Materials	Al	Mo	Sn	Zr	Cr	V	C	H	O	N	Ti
Ti-6Al-4V	6.29	-	-	-	-	4.02	0.062	0.012	0.15	0.015	Bal.
Ti-622222	5.93	2.04	1.97	2.03	2.00	1.99	0.01	0.001	0.04	0.01	Bal.

The LDM test was conducted by using the LDM800 laser additive manufacturing system, which is equipped with an IPG 6.0 kW fiber laser, three axis motion system, synchronous powder feeding system and argon protection box, as shown in Fig. 1. The LDM test was carried out in the Ar atmosphere with O_2 content less than 50 ppm. Basing on the preliminary test results, the optimized process parameters for LDM test were selected as listed in Table 2. In addition, the laser deposition process was conducted in the manner of short side one-way reciprocation with the designed thickness of 0.8 mm for each layer [29].

Table 2
Process parameters for LDM test

Laser power	Scan speed	Scan spacing	Feeding rate	Spot diameter
2400 W	10 mm/s	2.3 mm	8 g/min	4 mm

The LDMed Ti-622222 alloy was subjected to solution and aging treatment. As shown in Table 3, three solution temperatures were selected to investigate the effect of solution temperature on microstructure and mechanical properties of LDMed Ti-622222 alloy, and to further determine the optimal heat treatment system.

Table 3
Parameters for solution and aging treatment

Heat treatment process	Solution treatment	Aging treatment
HT-1	900 ℃/2 h, air cooling	540 ℃/4 h, air cooling
HT-2	920 ℃/2 h, air cooling	
HT-3	940 ℃/2 h, air cooling	

The metallographic samples of as-deposited and heat-treated were prepared according to the standard procedures [29] and etched by the Kroll corrodent (HF: HNO_3: H_2O, volume ratio 1:6:7). The microstructure of LDMed samples was observed and analyzed by the GX51 OLYMPUS optical microscopy (OM) and JSM-7001F scanning electron microscope (SEM).

The microhardness of LDMed Ti-622222 alloy was measured on the polished surface using a HVS-1000A Vickers hardness tester. The load was set as 500 g and the pressure retention time was 10 s. In order to ensure the accuracy of the data, the close range should be measured for many times during the experiment, and the average value was recorded as the microhardness value of the material.

The tensile tests of LDMed samples were carried out at room temperature by using the INSTRON 5982 universal electronic machine. The sampling direction of tensile sample was perpendicular to the deposition direction (XY direction) as shown in Fig. 2(a) with the dimension shown in Fig. 2(b). The tensile tests were repeated three times for each condition and the average value was recorded as the property values of the material. All the tensile measurements were performed according to the standard of BS EN ISO 6892-1: 2016 [30].

The impact tests of LDMed samples were carried out at room temperature by using the JB-30B impact tester. The pendulum energy was set as 300 J. The impact sample was sampled along the deposition direction (Z direction) and vertical deposition direction (XY direction), respectively. The dimension of impact samples was shown in Fig. 2(c). Three impact samples were taken for each sampling direction to ensure the value stable.

3 Results And Discussion

3.1 Microstructure analysis

Figure 3 shows the morphology of as-deposited LDMed Ti-622222 alloy. It can be found in macrostructure (Fig. 3(a)) that the adjacent deposited layers are in metallurgical bonding state showing obvious layer band. The epitaxial growth coarse β columnar grains can also be observed, and the adjacent β columnar grains alternate between light and dark due to the different orientations of the grains in the structure [31]. These β columnar grains basically grow along the deposition direction and slightly tilt in the scanning direction of laser beam. During the laser deposition process, the temperature gradient is usually along the deposition direction due to the lower temperature for the substrate. Therefore, the solidification process starts from the substrate side, and the nucleation grows mainly along the direction of the maximum temperature gradient according to the crystal growth theory [32]. Moreover, the growth of β columnar crystals along the deposition direction is continuous as shown in Fig. 3(b), which is due to the deposition characteristic of layer by layer and the metallurgical bonding for interlayer for laser deposition manufacturing. It can be found in Fig. 3(c) that the fine basket-weave structure evenly distributes within the coarse β columnar crystals. The basket-weave structure consists of large numbers of disoriented and elongated α phases and a small amount of interphase β phases, which are staggered. The proportion of α phase is much higher than that of β phase. In addition, it can be observed that the grain boundaries are intact and there exists a large number of α lamella around the grain boundaries, which grow into clusters along the grain boundaries. During the laser deposition process, the formation of present deposited layer may produce the effect of reheat and even remelting on the last deposited layer. Thus, the internal structure for the LDMed Ti-622222 alloy is subjected to rapid heating and cooling for many times. In this

case, the β phases in the microstructure rapidly transforms into α phases and the large numbers of primary α phases will be rapid growth with elongated shape. Therefore, the microstructure of the as-deposited sample is fine and the volume fraction of α phase is significantly greater than that of β phase [33, 34].

Figure 4 shows the microstructure of the LDMed Ti-622222 alloy after heat treatment. It can be seen that the microstructure of the heat-treated Ti-622222 alloy changes obviously compared with that of as-deposited alloy shown in Fig. 3(c). After the solution and aging treatment, the microstructure is still composed of the basket-weave structure knitted with α phase and β phase, but the phase morphology of LDMed Ti-622222 alloy change dramatically with the solution temperature increasing. This is mainly caused by the process of α + β/β phase transition at high temperature. It has been reported that [35] the content of comprising elements for Ti alloy can affects (α + β)/β phase transition point ($T_{\alpha+\beta/\beta}$) according to the following formula:

$$T_{\alpha+\beta/\beta}=885\ ^{\circ}\mathrm{C}+\sum(C_i \times \eta_i)$$

where C_i represents the content of i element, and η_i is on behalf of the effect of i element content on α + β/β phase transformation point. Based on the chemical component of Ti-622222 alloy listed in Table 1 and the measured η_i value [29], the value of $T_{\alpha+\beta/\beta}$ for Ti-622222 alloy calculated by the formula is about 940 ℃. When the solution temperature is 900 ℃ lower than the $T_{\alpha+\beta/\beta}$, the solution process is carried out within the two-phase region of α + β. In this case, the partial primary α phases transforms into β phases. And then small amounts of elongated secondary α phases are precipitated in the β phase matrix in the subsequent aging process, as shown in Fig. 4(a). And due to the high temperature, the residual primary α phases grows obviously showing the shape of rod-like with lower length-width ratio. In the condition of HT-2, more primary α phase have transformed into β phases during the solution process, which finally leads to the decrease in the content of short rod-like primary α phases. Finally, more fine secondary α phases precipitate during the aging process, as shown in Fig. 4(b). When the solution temperature reaches the $T_{\alpha+\beta/\beta}$ (940 ℃), almost all the primary α phases transform into β phases, and then secondary α phases fully precipitate and grow up in the β phase matrix during the aging process. Therefore, the microstructure at room temperature is composed of elongated lamellar secondary α phases and interphase β phases as shown in Fig. 4(c).

3.2 Microhardness analysis

The average microhardness of LDMed Ti-622222 alloy with different solution and aging treatments are shown in Fig. 5. It can be seen that the solution and aging treatment has significant effects on the microhardness of LDMed Ti-622222 alloy. The average microhardness of the as-deposited Ti-622222 alloy is only 569.5 $HV_{0.2}$, which is much lower than that of the heat-treated alloy. Moreover, the microhardness of LDMed Ti-622222 alloy shows a rising trend with the solution temperature increasing. It is mainly because that with the solution temperature increasing, more α phases transforms into β phases, which promotes the precipitation of secondary α phases with small size during the aging process

(Fig. 4). The fine secondary α phases produce distinct fine-grained strengthening effect resulting in the microhardness increasing. In addition, in the condition of HT-3, the secondary α phases fully precipitate and grow into thin lamellar phases (shown in Fig. 4(c)) with poor compatible deformation capability compared with primary α phases, which may also result in the microhardness increasing of LDMed Ti-622222 alloy after HT-3 treatment.

3.3 Tensile property analysis

The tensile properties derived from the the stress-strain curves for LDMed Ti-622222 alloy before and after solution and aging treatment are shown in Fig. 6. It can be seen that for the as-deposited Ti-622222 alloy, the average ultimate strength (σ_b) is 1025 MPa and the average yield strength ($\sigma_{0.2}$) is 943 MPa, which is higher than the tensile results for LDMed TC4 alloy reported by other literature [36]. For plasticity, the elongation (δ) is 6.0% and the reduction of area (ψ) is 14.7%. By contrast, there is an obvious increase in strength for Ti-622222 alloy after the solution and aging treatment. Moreover, the strength increases with the solution temperature increasing. The LDMed Ti-622222 alloy after HT-3 treatment exhibits the highest σ_b value (1197.4 MPa) and $\sigma_{0.2}$ value (1080.7 MPa). On the contrary, the plasticity (δ and ψ) decreases with the solution temperature increasing, and the optimum plasticity (δ: 7.8%; ψ: 19.2%) is obtained by the LDMed Ti-622222 alloy after HT-1 treatment.

The variation of tensile properties for LDMed Ti-622222 alloy closely depends on its microstructure. After solution and aging treatment, the primary α phase decreases but the fine secondary α phase increases (Fig. 4). The precipitation of fine secondary α phase leads to the increase in intergranular boundaries, which can hinder the dislocation slip improving the strength. Therefore, the strength for LDMed Ti-622222 alloy after heat treatment is higher than that of as-deposited alloy and increases with the solution temperature increasing. In addition, the plastic deformation ability of the primary α phase with short rod shape is stronger than that of the lamellar secondary α phase. Therefore, with the solution temperature increasing, the precipitation of lamellar secondary α phase increases leading to the decreasing of plasticity of LDMed Ti-622222 alloy. It is well known that there exists the anisotropy of tensile property in different sampling sections for LDMed samples due to the microstructure anisotropy [28]. Therefore, it can be deduced that the LDMed Ti-622222 alloy in scanning direction exhibits higher strength but lower plasticity than that of sample in deposition direction due to the more grain boundary for β columnar grain in scanning direction (Fig. 3(b)) [28, 29].

Figure 7 shows the tensile fracture morphology of the LDMed Ti-622222 alloy before and after heat treatment. In macroscopic view (Fig. 7(a)-(d)), LDMed Ti-622222 alloys before and after heat treatment all show obvious cleavage appearance formed by the brittle fracture of α/β lamellae, which indicates the brittle characteristics corresponding to the low plasticity [36]. By contrast, the tensile sample after HT-1 treatment exhibits obvious neck shrinkage (Fig. 7(b)) indicating the relatively superior plasticity. The micro-fractography is well related with the plasticity value for tensile property (Fig. 6(b)). In microscopic view (Fig. 7(e)-(h)), numerous fine dimples distribute on the fracture surface indicating that the LDMed Ti-622222 alloys are involved the ductile fracture mechanism [37]. Generally, LDMed samples would

inevitably produce certain hole defects after powders were melted and solidified, which may be caused by unmelted powder or gas. Previous report has shown that the existence of microvoids contributes to improve plasticity of the material [38]. The analysis result of fracture morphology shows that the fracture mechanism of the LDMed Ti-622222 alloys is a mixture of ductile and brittle fracture.

3.4 Impact property analysis

Figure 8 shows the impact properties of LDMed Ti-622222 alloy. It can be seen that the average impact toughness of the impact sample in scanning direction is 23.4 J/cm^2, lower than that in deposition direction (40.9 J/cm^2). The obvious anisotropy of impact property depends on the microstructure characteristics in different sampling direction. During the impact process, the impact load is parallel to the growth direction of β columnar grain for the impact sample in scanning direction, but perpendicular to the growth direction of β columnar grain for the impact sample in deposition direction. Compared with the impact sample in scanning direction, the impact sample in deposition direction needs to overcome more grain boundaries during the fracture process, and then can consume more energy during the impact process. Therefore, the impact toughness of the sample in deposition direction is higher than that in scanning direction.

Compared with as-deposited samples, the impact toughness of the LDMed Ti-622222 alloy is improved after solution and aging treatment. With the solution temperature increasing, impact toughness first increases and then decreases. By contrast, the fluctuation of impact toughness for sample in scanning direction is larger than that in deposition direction. Toughness is the comprehensive expression of material strength and plasticity, which is closely related to the microstructure characteristics. After solution and aging treatment, the microstructure has been significantly refined due to the precipitation of lamellar secondary α phases (Fig. 4), which promotes the impact toughness increase. In addition, the heat treatment can eliminate the residual stress generated in the process of laser deposition and reduce the internal defect of the sample to some extent, which can also improve the impact toughness.

Figure 9 shows the impact fracture morphology of the LDMed Ti-622222 alloy in scanning direction before and after heat treatment. In macroscopic view (Fig. 9(a)-(d)), LDMed Ti-622222 alloys before and after heat treatment all show obvious cleavage appearance indicating the brittle characteristics. In microscopic view (Fig. 9(e)-(h)), numerous fine dimples distribute on the fracture surface indicating the ductile characteristics. In contrast, the fracture undulate is larger and the dimples are deeper for the impact samples after HT-1 and HT-2 treatment, indicating that the samples absorb more energy during the impact fracture process and have higher impact toughness.

Figure 10 shows the impact fracture morphology of the LDMed Ti-622222 alloy in deposition direction before and after heat treatment. Its variation tendency is in agreement with that in scanning direction (Fig. 9). Compared with impact samples in scanning direction, at the same solution temperature, the cleavage content is lower and the dimples of the impact samples in deposition direction are larger and deeper, which leads to the better toughness.

By comprehensive analysis of the impact performance data and fracture morphology, it is known that the specimen has relatively excellent impact performance when the solution temperature is 920 ℃.

4 Conclusions

In this paper, a newly developed Ti-622222 alloy was fabricated by the laser deposition manufacturing, and the solution and aging treatment was carried out. The microstructure and mechanical properties of LDMed Ti-622222 alloy before and after heat treatment were deeply analyzed. The obtained conclusions were as follows:

(1) The as-deposited Ti-622222 alloy is composed of coarse β columnar grains, which is approximately parallel to the deposition direction. The basket-weave structure consisting of large numbers of elongated α phases and a small amount of interphase β phases is distributed within the β columnar grain.

(2) Solution and aging treatment have a marked impact on microstructure of LDMed Ti-622222 alloy. With the solution temperature increasing, the size and content of primary α phase decrease, but the fine secondary α phase increases.

(3) The microhardness of LDMed Ti-622222 alloy shows a rising trend with the solution temperature increasing due to the fine-grained strengthening effect caused by the precipitation of fine secondary α phases.

(4) The LDMed Ti-622222 alloy exhibits superior tensile strength (1025 MPa) and inferior elongation (6.0%). With the solution temperature increasing, the strength gradually increases but the plasticity first increases and then decreases. The LDMed Ti-622222 alloy exhibits a mixed fracture mechanism of ductile and brittle fracture.

(5) The LDMed Ti-622222 alloy exhibits obvious anisotropy of impact property, the average impact toughness of the impact sample in scanning direction is 23.4 J/cm^2, lower than that in deposition direction (40.9 J/cm^2). After solution and aging treatment, the impact toughness improves significantly. With the solution temperature increasing, impact toughness first increases and then decreases.

Declarations

a. Funding

The authors very much appreciate the financial supports from the Liaoning Province Department of Education fund [Grant No. JYT2020061 and JYT2020048], the Open Fund of Key Laboratory of Fundamental Science for National Defense of Aeronautical Digital Manufacturing Process of Shenyang Aerospace University [Grant No. SHSYS202001], the Scientific Research Start-up Fund for the Talents Introduction of Shenyang Aerospace University [Grant No. 19YB40].

b. Competing interests

The authors declared that they have no conflicts of interest to this work. We declare that we do not have any commercial or associative interest that represents a conflict of interest in connection with the work submitted.

c. Availability of data and material

Data is available upon request. We will also deposit it to a repository after acceptation.

d. Code availability

Not applicable.

e. Ethics approval

Not applicable. This research is on LDM experimentation, it does not need Institutional Review Board (IRB) approval.

f. Consent to participate

Not applicable.

g. Consent for publication

The authors give our consent for the publication of identifiable details, which can include photograph(s) and details within the text (“Material”) to be published in the International Journal of Advanced Manufacturing Technology.

h. Authors' contributions

Jiabao Wu and Shuai Shao carried out the LDM experimentation. Chao Wang and Junzhen Yi analyzed the data, and wrote/revised the manuscript. Jiaxing Wang carried out the experiments of mechanical property and proofread the manuscript. Linyun Qin and Guang Yang conceptualized the experiment, reviewed and revised the manuscript.

References

1. Cen MJ, Liu Y, Chen X, Zhang HW, Li YX (2019) Inclusions in melting process of titanium and titanium alloys. China Foundry 16(4):223–231
2. Prem AM, Ramesh R (2017) Sliding wear characteristics of solid lubricant coating on titanium alloy surface modified by laser texturing and ternary hard coatings. T Nonferr Metal Soc 27(04):839–847
3. Boyer RR (1996) An overview on the use of titanium in the aerospace industry. Mater Sci Eng A 213:103–114
4. Bania PJ (1994) Beta Titanium Alloys and Their Role in the Titanium Industry. JOM 46(7):16–19

5. Li D, Hui SX, Ye WJ, Li CL (2016) Microstructure and mechanical properties of a new high-strength and high-toughness titanium alloy.Rare Metals1–7
6. Li CL, Mi XJ, Ye WJ, Hui SX (2016) A Study on Microstructures and Properties of A high Strength/Toughness Ti-3Al-1Fe-4V-4.5Cr Alloy. Proceedings of the 13th World Conference on Titanium. John Wiley & Sons, Inc. 563–568
7. Zhou W, Ge P, Zhao YQ, Xin SW, Li Q, Wang J, Huang CW, Chen J (2017) Relationship between Mechanical Properties and Microstructure in a New High Strength β Titanium Alloy. Rare Metal Mat Eng 46(8):2076–2079
8. Liu A, Wang L, Dai H (2018) Effect of Heat Treatment on the Microstructure and Dynamic Behavior of Ti-10V-2Fe-3Al Alloy. Mater Sci Forum 910:155–160
9. Ratochka IV, Mishin IP, Lykova ON, Naydenkin EV (2018) Effect of annealing on the superplastic properties of ultrafine-grained Ti-5Al-5V-5Mo-1Cr-1Fe alloy. Mater Sci Eng A 803:140511
10. Wang QR, Sha AX, Huang LJ, Li XW, Mi GB (2019) Double Annealing Processes of Ti-5Al-5Mo-5V-1Cr-1Fe Titanium Alloy.Mater Sci Forum33–37
11. Liu ZD, Du ZX, Jiang HY, Gong TH, Cui XM, Liu JW, Cheng J (2021) Microstructure evolution and corresponding tensile properties of Ti-5Al-5Mo-5V-1Cr-1Fe alloy controlling by multi-heat treatments. Prog Nat Sci-Mater 31:731–741
12. Moiseyev VN (2006) Titanium alloys, Russian aircraft and aerospace application. Taylor&Francis Group, London
13. Harper M, Williams R, Viswananthan GB (2003) The effect of heat treatment on the mi-crostructure of Ti-5Al-5Mo-5V-3Cr-1Fe (Ti-555). Ti-2003 Science and Technology. DGM, Hamburg, p 1559
14. Fanning JC (2005) Properties of TIMETAL 555 (Ti-5Al-5Mo-5V-3Cr-0.6Fe). J Mater Eng Perform 14(6):788–791
15. Li J, Wang HM (2013) Aging response of laser melting deposited Ti-6Al-2Zr-1Mo-1V alloy. Mater Sci Eng A 560:193–199
16. Hu YB, Cong WL (2018) A review on laser deposition-additive manufacturing of ceramics and ceramic reinforced metal matrix composites. Ceram Int 44:20599–20612
17. Bohlen A, Freibe H, Hunkel M, Vollertsen F (2018) Additive manufacturing of tool steel by laser metal deposition. Procedia CIRP 74:192–195
18. Ge P, Zhang Z, Tan ZJ, Hu CP, Zhao GZ, Guo X (2019) An integrated modeling of process-structure-property relationship in laser additive manufacturing of duplex titanium alloy. Int J Therm Sci 140:329–343
19. Zhang Q, Chen J, Tan H, Lin X, Huang WD (2016) Microstructure evolution and mechanical properties of laser additive manufactured Ti-5Al-2Sn-2Zr-4Mo-4Cr alloy. T Nonferr Metal Soc 26:2058–2066
20. Schwab H, Palm F, Kuhn U, Eckert J (2016) Microstructure and mechanical properties of the near-beta titanium alloy Ti-5553 processed by selective laser melting. Mater Des 105:75–80

21. Liu CM, Tian XJ, Wang HM, Liu D (2014) Obtaining bimodal microstructure in laser melting deposited Ti-5Al-5Mo-5V-1Cr-1Fe near β titanium alloy. Mater Sci Eng A 609:177–184
22. Liu CM, Wang HM, Tian XJ, Tang HB, Liu D (2013) Microstructure and tensile properties of laser melting deposited Ti-5Al-5Mo-5V-1Cr-1Fe near β titanium alloy. Mater Sci Eng A 586:323–329
23. Liu CM, Wang HM, Tian XJ, Tang HB (2014) Subtransus triplex heat treatment of laser melting deposited Ti-5Al-5Mo-5V-1Cr-1Fe near β titanium alloy. Mater Sci Eng A 590:30–36
24. Chen F, Xu G, Zhang X, Zhou K (2016) Exploring the Phase Transformation in β-Quenched Ti-55531 Alloy During Continuous Heating via Dilatometric Measurement, Microstructure Characterization, and Diffusion Analysis. Metall Mater Trans A 47:5383–5394
25. Deng H, Chen LQ, Qiu WB, Zheng Z, Tang Y, Hu ZD (2019) Microstructure and mechanical properties of as-deposited and heat treated Ti-5Al-5Mo-5V-3Cr-1Zr (Ti-55531) alloy fabricated by laser melting deposition. J Alloys Compd 810:151792
26. Wei YQ, Xia ZX, Le GM, Tang J, Cui XD (2019) Microstructure and mechanical properties of as-deposited and heat treated Ti-5Al-5Mo-5V-3Cr-1Zr (Ti-55531) alloy fabricated by laser melting deposition. J Alloys Compd 810:151792
27. Chen ZQ, Xu LJ, Liang ZQ, Cao SZ, Yang JK, Xiao SL, Tian J, Chen YY (2021) Effect of solution treatment and aging on microstructure, tensile properties and creep behavior of a hot-rolled β high strength titanium alloy with a composition of Ti-3.5Al-5Mo-6V-3Cr-2Sn-0.5Fe-0.1B-0.1C. Mater Sci Eng A 823:141728
28. Li RK, Wang HM, He B, Li Z, Zhu YY, Zheng DD, Tian XJ, Zhang SQ (2021) Effect of α texture on the anisotropy of yield strength in Ti-6Al-2Zr-1Mo-1V alloy fabricated by laser directed energy deposition technique. Mater Sci Eng A 824:141771
29. Wang C, Yi JZ, Qin LY, Wang WD, Wang XM, Yang G (2019) Effects of double annealing on microstructure and mechanical properties of laser melting deposition TA15 titanium alloy. Mater Res Express 6:116526
30. BS EN ISO 6892-1 (2016) : Metallic materials-Tensile testing-Part 1: Method of test at room temperature, 2016
31. Zhu YY, Liu D, Tian XJ, Tang HB, Wang HM (2014) Characterization of microstructure and mechanical properties of laser melting deposited Ti-6.5Al-3.5Mo-1.5Zr-0.3Si titanium alloy. Mater Des 56:445–453
32. Liu FC, Lin X, Huang CP, Song MH, Yang GL, Chen J, Huang WD (2011) The effect of laser scanning path on microstructures and mechanical properties of laser solid formed nickel-base superalloy Inconel 718. J Alloys Compd 509(13):450545
33. Zhu YY, Tian XJ, Li J, Wang HM (2014) Microstructure evolution and layer bands of laser melting deposition Ti-6.5Al-3.5Mo-1.5Zr-0.3Si titanium alloy. J Alloys Compd 616:468–474
34. Ren HS, Tian XJ, Liu D, Liu J, Wang HM (2015) Microstructural evolution and mechanical properties of laser melting deposited Ti-6.5Al-3.5Mo-1.5Zr-0.3Si titanium alloy. T Nonferr Metal Soc 25:1856–1864

35. Leyens C, Peters M (2003) Titanium and titanium alloys. WILEY-VCH Verlag GmbH & Co. KGaA, Weinheim
36. Zhou X, Xu DK, Geng SJ, Fan YQ, Liu MX, Wang Q, Wang FH (2021) Mechanical properties, corrosion behavior and cytotoxicity of Ti-6Al-4V alloy fabricated by laser metal deposition. Mater Charact 179:111302
37. Huang SX, Zhao YQ, Yu JS, Lin C, Wu C, Jia WJ (2020) Partition of Nb element on microstructure, tensile and impact properties of a near α Ti-4Nb alloy. J Alloys Compd 826:154128
38. Wang M, Song B, Wei Q, Zhang Y, Shi Y (2019) Effects of annealing on the microstructure and mechanical properties of selective laser melted AlSi7Mg alloy. Mater Sci Eng A 739:463–472

Figures

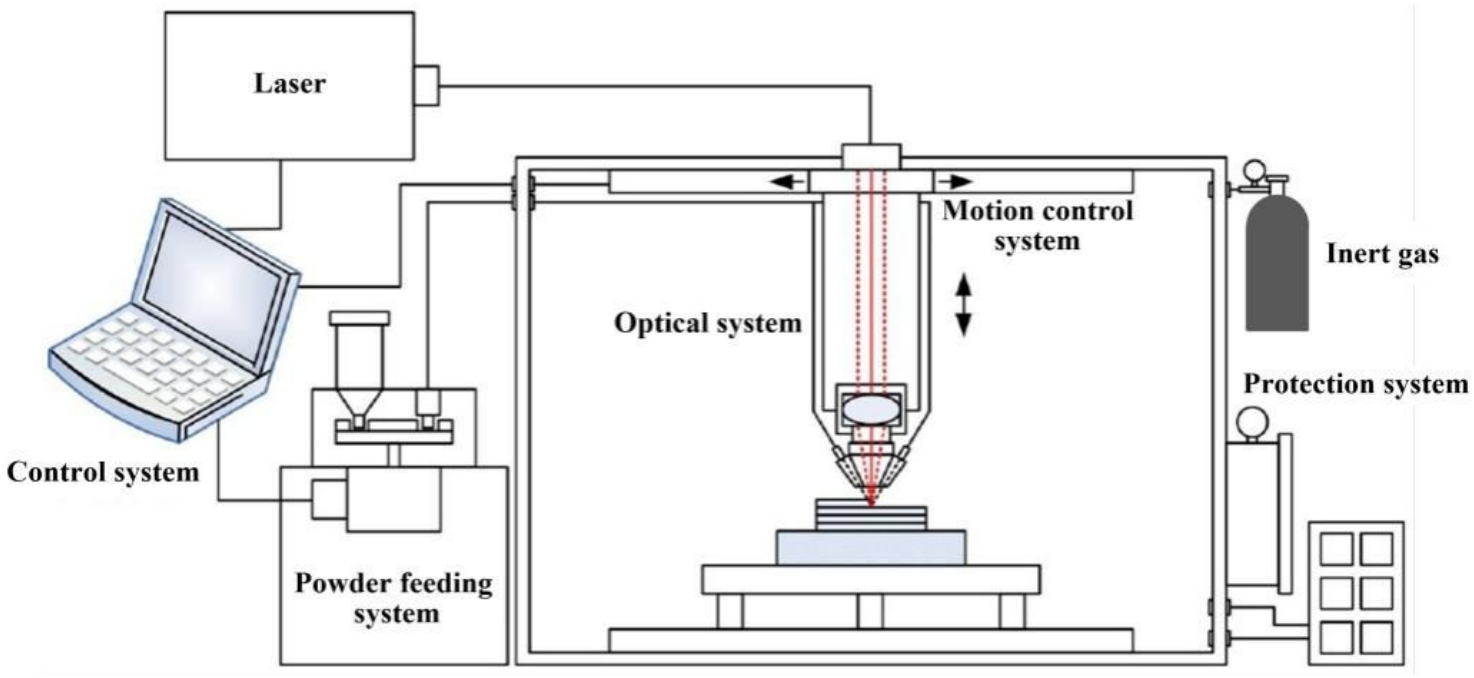

Figure 1

Schematic of laser additive manufacturing system used in this work

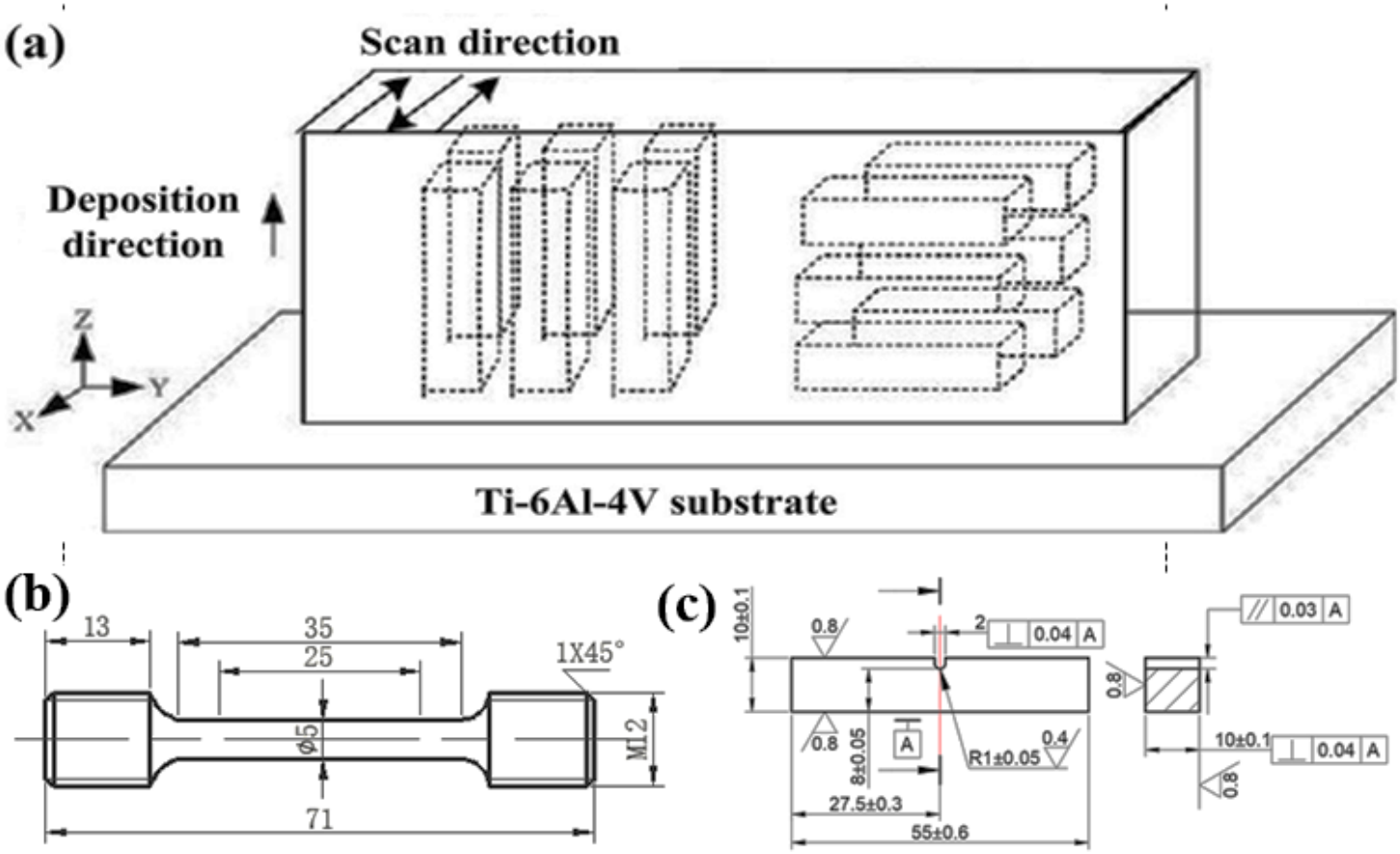

Figure 2

Sampling and dimension schematic of samples for mechanical property tests: (a) Sampling schematic; (b) dimension schematic of tensile sample; (c) dimension schematic of impact sample

Figure 3

Morphology of as-deposited Ti-622222 alloy

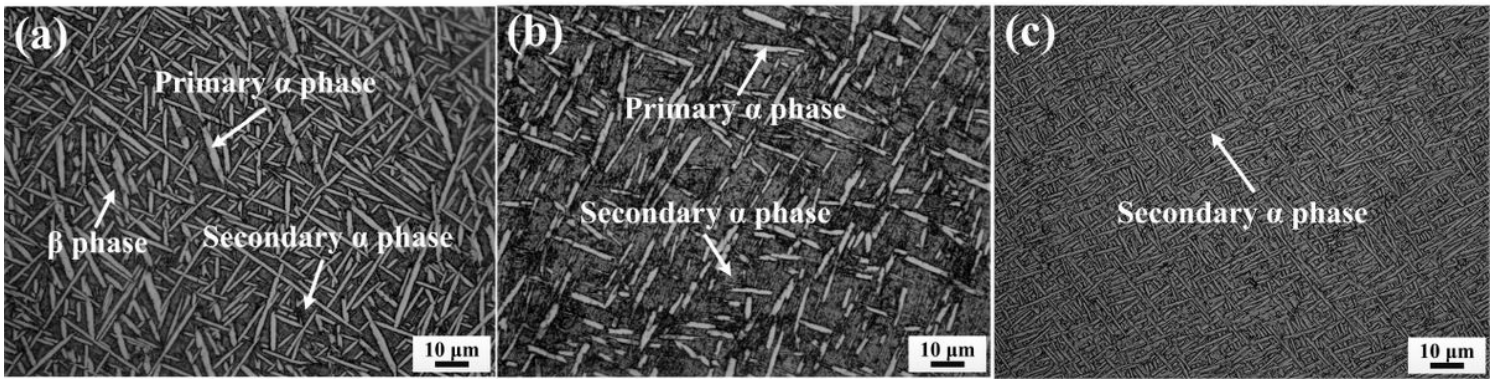

Figure 4

Microstructure of LDMed Ti-622222 alloy after heat treatment: (a) HT-1; (b) HT-2; (c) HT-3

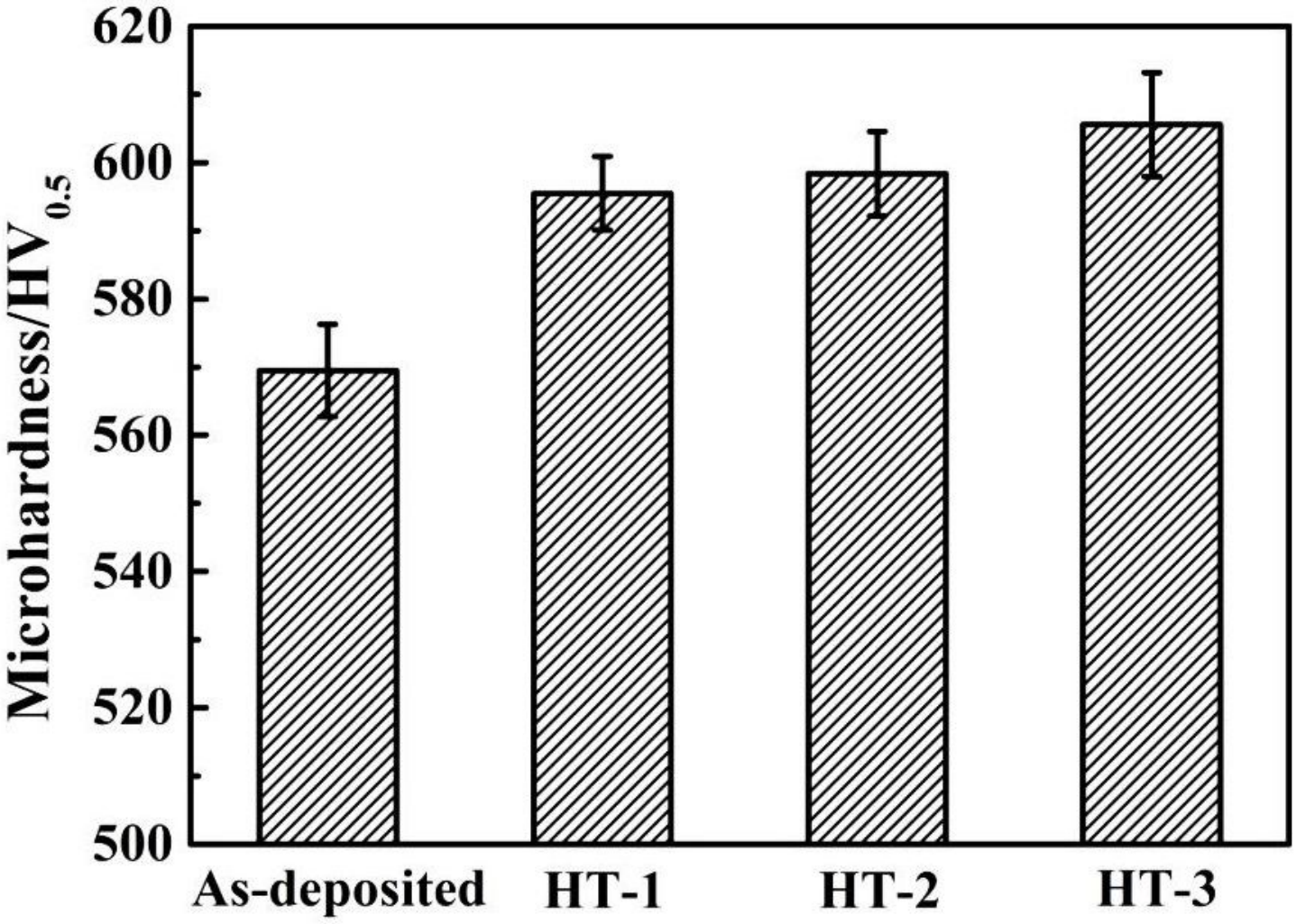

Figure 5

Microhardness of LDMed Ti-622222 alloy

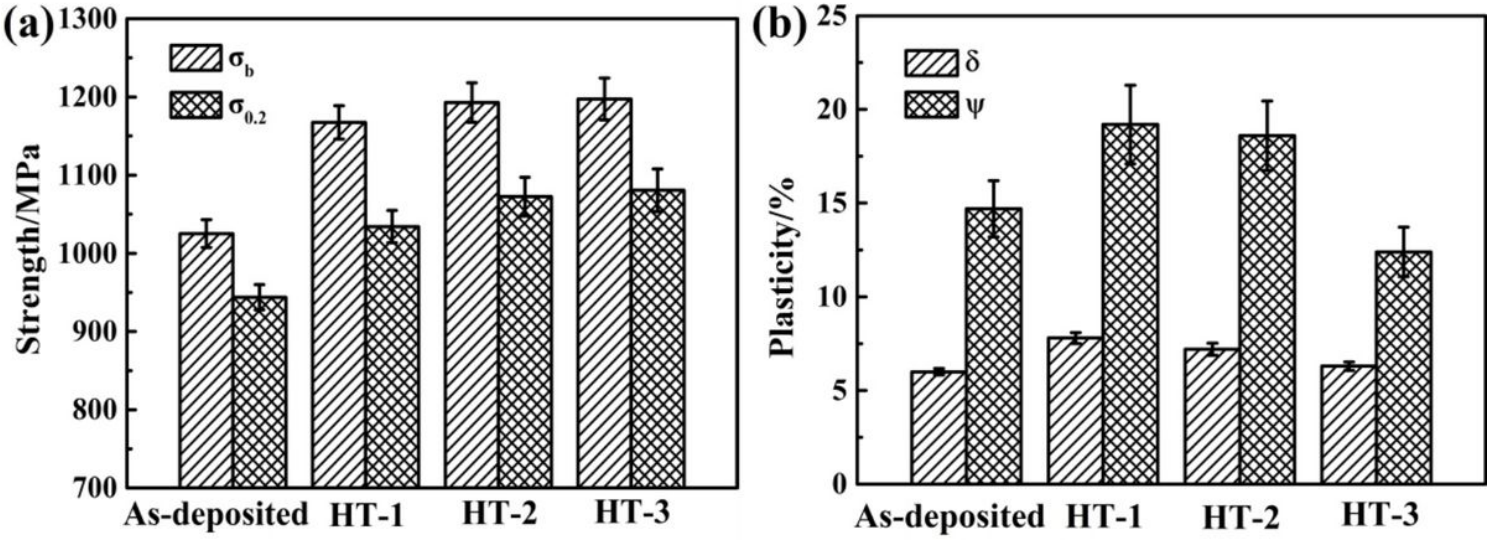

Figure 6

Tensile properties for LDMed Ti-622222 alloy: (a) strength; (b) plasticity

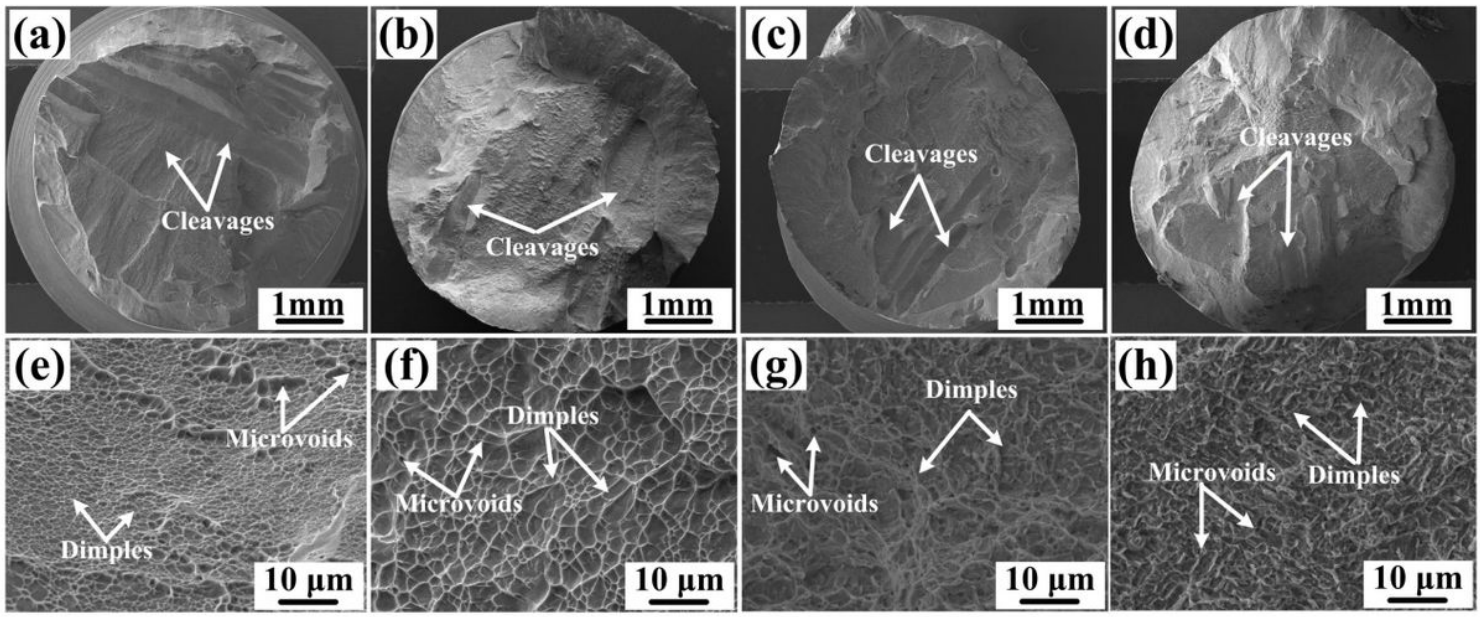

Figure 7

Fracture morphology of tensile sample for LDMed Ti-622222 alloy

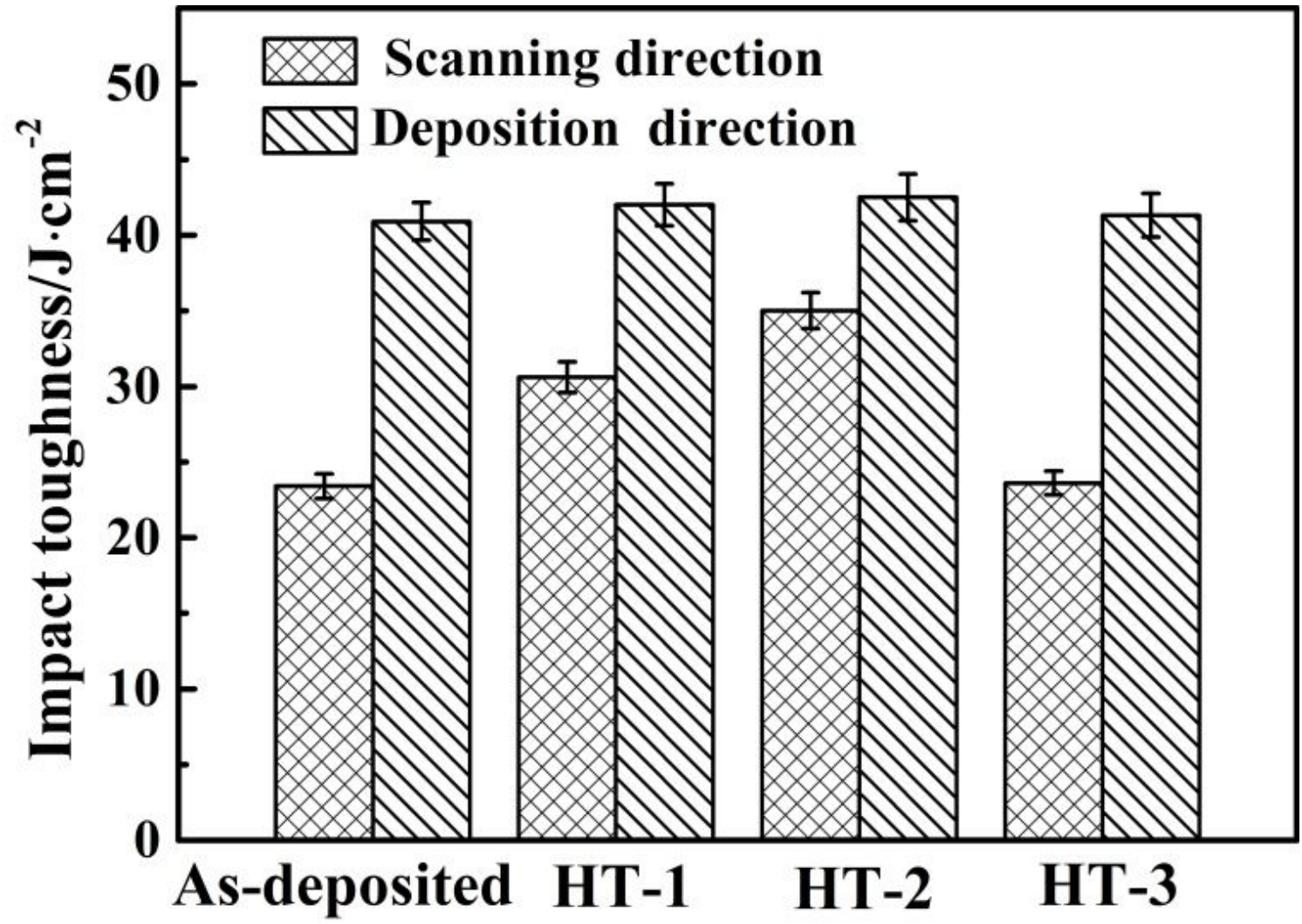

Figure 8

Impact property for LDMed Ti-622222 alloy

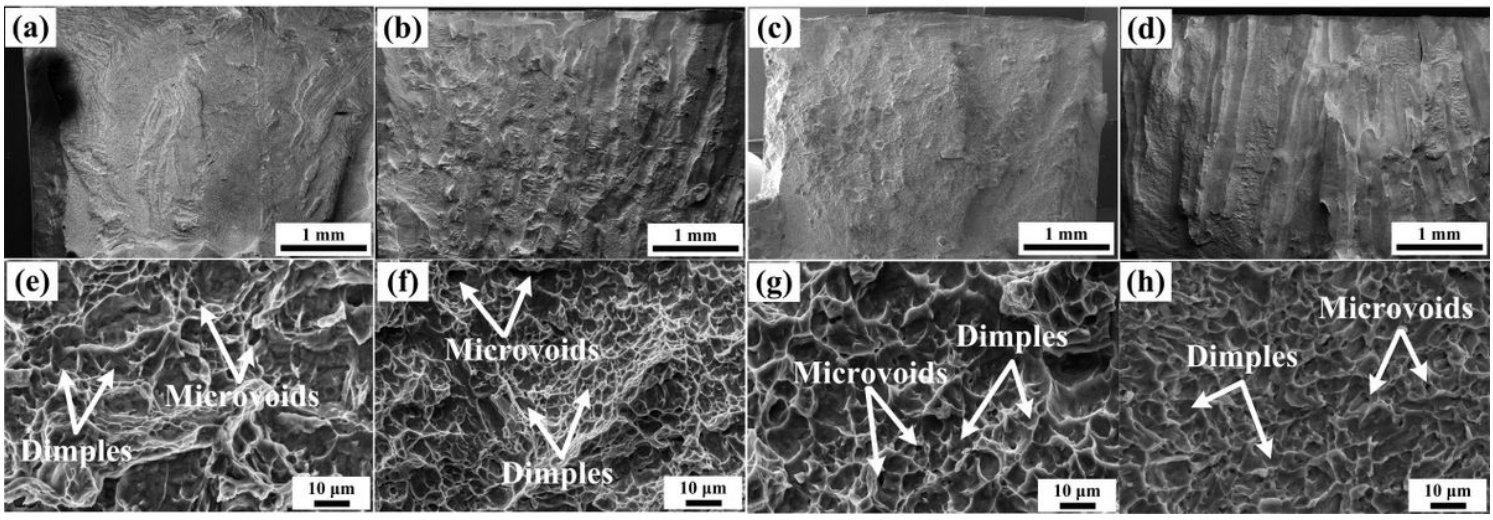

Figure 9

Fracture morphology of impact samples in scanning direction for LDMed Ti-622222 alloy: (a), (e) as-deposited; (b), (f) HT-1; (c), (g) HT-2; (d), (h) HT-3

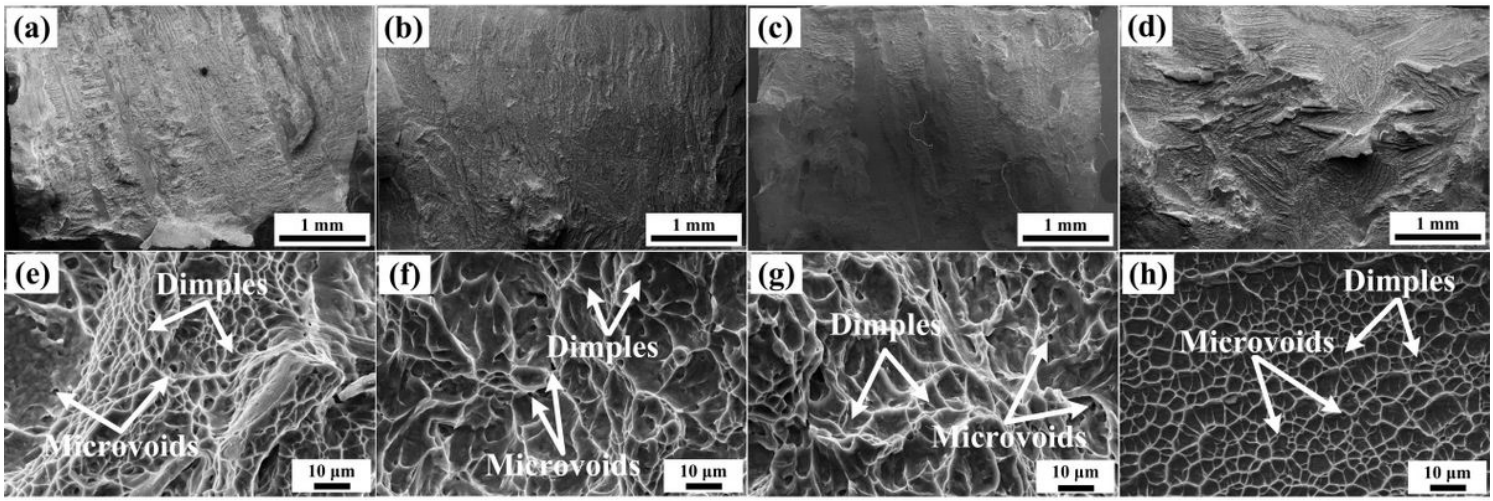

Figure 10

Fracture morphology of impact samples in deposition direction for LDMed Ti-622222 alloy: (a), (e) as-deposited; (b), (f) HT-1; (c), (g) HT-2; (d), (h) HT-3